

## Gallium arsenide phosphide grown by close-spaced vapor transport from mixed powder sources for low-cost III-V photovoltaic and photoelectrochemical devices

Ann L. Greenaway,<sup>a</sup> Allison L. Davis,<sup>b</sup> Jason W. Boucher,<sup>c</sup> Andrew J. Ritenour,<sup>a</sup> Shaul Aloni<sup>d</sup>  
and Shannon W. Boettcher\*<sup>a</sup>

<sup>a</sup>Department of Chemistry and Biochemistry, University of Oregon, Eugene, Oregon, 97403,  
USA. Email: [swb@uoregon.edu](mailto:swb@uoregon.edu)

<sup>b</sup>Department of Natural and Physical Sciences, Park University, Parkville, Missouri, 64152,  
USA.

<sup>c</sup>Department of Physics, University of Oregon, Eugene, Oregon, 97403, USA.

<sup>d</sup>The Molecular Foundry, Lawrence Berkeley National Laboratory, Berkeley, California, 94720,  
USA.

### Supporting Information

#### 1. Details of pellet production for GaAs<sub>1-x</sub>P<sub>x</sub> film growth

Mixed GaAs and GaP powder sources were produced by determining the target composition, then grinding each material separately before combining in a pellet die in the appropriate ratio. The target composition for each source pellet used in this study is given below.

**Table S1:** Details of pellet compositions, resulting film compositions, and thicknesses of the resulting films (averaged for the four  $T_{\text{src}} = 900$  °C samples for the temperature series).

Series	Sample	Pellet [P] (atom %)	Film [P] by XRD (atom %)	Difference (%)	Film thickness for 900 °C films (μm)
Varied Composition	C1	33.7	31.4	7.0	12 ± 4
	C2	39.6	36.1	9.0	4.7 ± 0.5
	C3	51.2	44.3	13.5	6 ± 1
	C4	60.9	52.1	14.3	7 ± 1
	C5	67.7	61.7	9.0	9 ± 3
Varied Temperature	Average for T1, T3, T5, T7, T9	29.5	28 ± 1	6.1	4.2 ± 0.5

## 2. Materials characterization

### 2.1 Pellet XRD analysis

Following the ten growths for the temperature series, XRD analysis on the pellet source showed almost complete sintering of the pellet to form a solid solution of  $\text{GaAs}_{0.7}\text{P}_{0.3}$ , as indicated by the dominance of peaks with intermediate  $d$  spacing to the GaAs and GaP reference peaks (from the International Crystal Structure Database) across the entire  $\theta/2\theta$  range (Fig. S1).

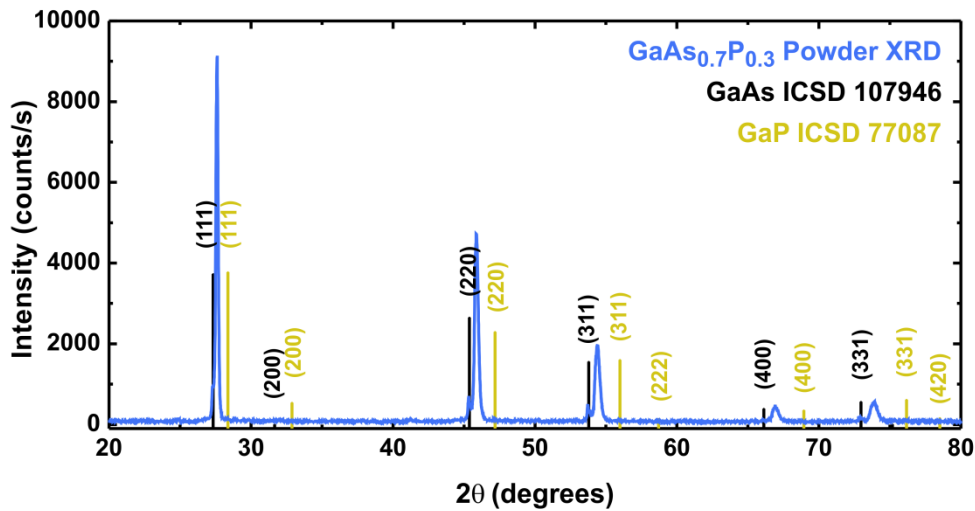


**Figure S1:** Powder XRD scan showing the analyzed pellet (blue) with the literature peak positions for GaAs and GaP shown (black and yellow, respectively).

### 2.2 Surface characterization for variable composition samples

The morphologies of the composition series films were characterized using SEM (FEI Helios Dual Beam). Because the pellets for this series did not undergo the extensive sintering as the temperature series pellet, all films showed a surface inhomogeneity including a high concentration of adventitious microstructures. Surface roughness was qualitatively seen to increase with [P] across the series, suggesting that lattice mismatch between the  $\text{GaAs}_{1-x}\text{P}_x$  film and the GaAs substrate also contributed.

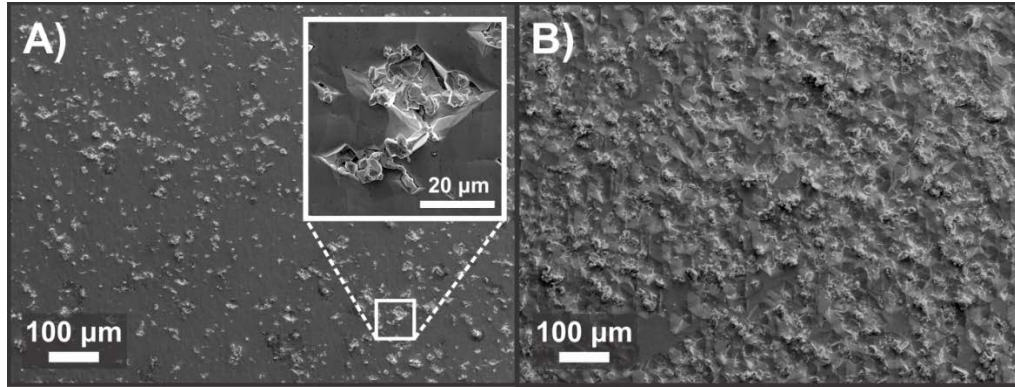


**Figure S2:** SEM images of composition series samples **A)** C1 [P] = 31%, with inset showing magnification of an adventitious microstructure and **B)** C5, [P] = 62% with many more microstructures and surface texturing as a result of the increased lattice mismatch from the substrate. These microstructures have been eliminated in the ~30% P samples by annealing of the source pellet, as shown in the main manuscript.

### 2.3 TOF-SIMS dopant concentrations

In order to determine [S] in the films and the source material for this study, the  $^{32}\text{S}$  peak was integrated for each film and compared to the integrated total counts for the  $^{69}\text{Ga}$  peak by converting counts to concentration using the RSF equation (1) in the main text. Due to the close incidence of the  $^{32}\text{S}$ ,  $\text{PH}_2$ , and  $\text{O}_2$  peaks in the mass spectra, some variance from  $N_{\text{D}}$  as measured by impedance spectroscopy is expected. We also note that the S concentration from SIMS seems to be higher in the films with more-defective surface morphologies. S may segregate to these defective regions and not contribute to the ionizable dopant concentration measured by impedance spectroscopy.

**Table S2:** Measured [S] in the two source GaP wafers and in a representative selection of GaAs<sub>1-x</sub>P<sub>x</sub> films.

Series	Sample	Film [P] by XRD (atom %)	[S] by TOF-SIMS (cm <sup>-3</sup> )
UW GaP Wafer*	--	--	$6.2 \times 10^{17}$
MTI GaP Wafer*	--	--	$4.7 \times 10^{16}$
Varied Composition	C1	31.4	$1.9 \times 10^{18}$
	C2	36.1	$1.2 \times 10^{18}$
	C4	52.1	$3.2 \times 10^{17}$
Varied Temperature	T1	30.2	$3.2 \times 10^{16}$
	T3	26.8	$4.3 \times 10^{17}$
	T5	26.0	$2.2 \times 10^{16}$
	T7	27.7	$3.4 \times 10^{16}$
	T9	27.5	$2.1 \times 10^{16}$

All concentrations calculated by referencing the total Ga count, rather than the total As count, which varies based on film P content. \* indicates that the GaP RSF, rather than GaAs, was used.<sup>1</sup>

### 3. Electronic characterization

#### 3.1 Absorption coefficients

Few literature reports exist on the absorption coefficients of the range of GaAs<sub>1-x</sub>P<sub>x</sub> compositions. For the temperature series and two composition series samples for which  $\Phi_{\text{int}}$  was fit to determine  $L_D$ , published absorption coefficients from Sukegawa et al.<sup>2</sup> were interpolated to match the measured interval of  $\Phi_{\text{int}}$ , and shifted in energy to match the exact band gap of the samples studied here.

**Table S3:** Interpolated values of  $\alpha(\lambda)$  from Hasegawa et al.<sup>2</sup>

[P] = 23 %		[P] = 38 %	
$\lambda$ (nm)	$\alpha(\lambda)$ (nm <sup>-1</sup> )	$\lambda$ (nm)	$\alpha(\lambda)$ (nm <sup>-1</sup> )
660	$1.78 \times 10^{-3}$	590	$1.9 \times 10^{-3}$
670	$1.68 \times 10^{-3}$	600	$1.76 \times 10^{-3}$
680	$1.59 \times 10^{-3}$	610	$1.63 \times 10^{-3}$
690	$1.49 \times 10^{-3}$	620	$1.52 \times 10^{-3}$
700	$1.40 \times 10^{-3}$	630	$1.42 \times 10^{-3}$
710	$1.31 \times 10^{-3}$	640	$1.31 \times 10^{-3}$
720	$1.23 \times 10^{-3}$	650	$1.19 \times 10^{-3}$
730	$1.13 \times 10^{-3}$	660	$1.01 \times 10^{-3}$
740	$8.25 \times 10^{-4}$	670	0
750	0		

### 3.2 Reflectivity measurements

The diffuse reflectance of each sample was measured using an integrating sphere, both bare and under a glass/acetonitrile stack in order to obtain the real reflectance which would be used to determine  $\Phi_{\text{int}}$ .<sup>3,4</sup> The measured reflectance values scaled between the known reflectances of GaP and GaAs, with the exception of C5, [P] = 62%, which showed a much lower reflectance as a result of its highly textured surface morphology (see Figure S2). For the varied temperature series, all samples showed approximately the same reflectance, with variations attributable to small differences in surface morphology.

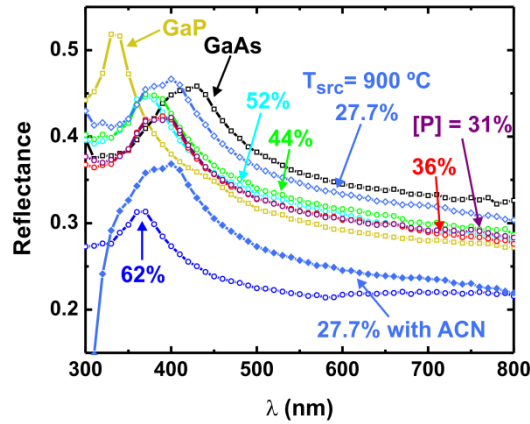


**Figure S3:** Measured reflectances in air of various  $\text{GaAs}_{1-x}\text{P}_x$  films, with GaAs and GaP reflectances shown for reference. The reflectance of T7, [P] = 27.7%, under the glass/acetonitrile stack is also shown (filled diamonds).

### 3.2 Spectral response control experiments

In order to confirm that there were no other contributions to the short-circuit nA signal, the  $\text{GaAs}_{1-x}\text{P}_x$  photoresponse to chopped 550 nm illumination was measured at 0 V and  $\pm 0.2$  V applied bias (Fig. S3). No dark current was measured at 0 V, with negligible dark current at -0.2 V. A 20 nA dark current was measured at +0.2 V, consistent with the slight voltage-dependent current observed in the  $J$ - $E$  measurements under simulated one-sun illumination.

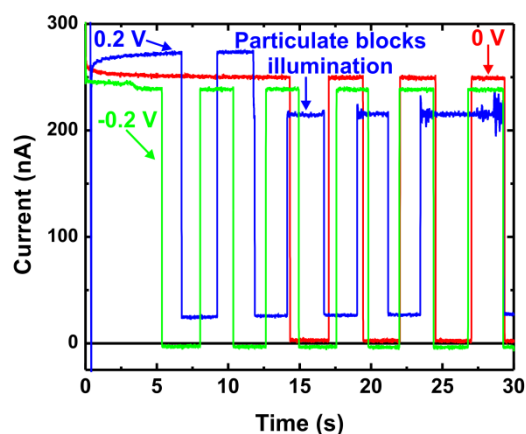


**Figure S4:** Chopped-light measurements at 0 V and  $\pm 0.2$  V in order to confirm that no additional current effected the measured spectral response signal under the low light measurement conditions used in the spectral response system.

### 3.3 Hall-effect Measurements

Hall effect measurements were made on a lab-built system with magnetic fields up to 10 kG. Mobilities were determined at 10 kG; dopant density uncertainties were determined by propagating the error associated with the standard deviation of film thicknesses (Table S2).

**Table S4:** Hall effect results for the temperature series samples grown on undoped substrates.

Sample	[P] (atom %)	$N_D$ ( $\text{cm}^{-3}$ )	$\mu_e$ ( $\text{cm}^2/\text{Vs}$ )
T8	28.1	$2.7 \times 10^{17} \pm 4 \times 10^{16}$	1010
T9	27.5	$1.3 \times 10^{17} \pm 3 \times 10^{16}$	1570
T10	27.7	$3.9 \times 10^{16} \pm 5 \times 10^{15}$	1100

### References

- 1 R. G. Wilson, F. A. Stevie and C. W. Magee, *Secondary ion mass spectrometry: a practical handbook for depth profiling and bulk impurity analysis*, Wiley, New York, 1989.
- 2 S. Hasegawa, A. Tanaka and T. Sukegawa, *J. Appl. Phys.*, 1984, **55**, 3188–3189.
- 3 A. J. Ritenour, R. C. Cramer, S. Levinrad and S. W. Boettcher, *ACS Appl. Mater. Interfaces*, 2012, **4**, 69–73.
- 4 A. J. Ritenour, J. W. Boucher, R. DeLancey, A. L. Greenaway, S. Aloni and S. W. Boettcher, *Energy Environ. Sci.*, 2015, **8**, 278–285.